COMPACT MIMO ANTENNA WITH ENHANCED ISOLATION FOR WLAN AND C-BAND APPLICATIONS

Trishna Doloi*[1], Gouree Shankar Das[1], Akash Buragohain[1,2], Partha Protim Kalita[1], and Yatish Beria[1]

[1]*Microwave Research Laboratory, Department of Physics, Dibrugarh University, Dibrugarh-786004, Assam, India*
[2]*Department of Physics, Tingkhong College, Dibrugarh-786612, Assam, India*

*Corresponding Author: doloitrishna1@gmail.com

(Received 25 September 2025; revised 5 January 2026; accepted 21 January 2026; published 1 August 2026)

Abstract: This article proposes a four-element Multiple Input Multiple Output (MIMO) antenna configuration to operate in the 4 - 8 GHz frequency range for WLAN and C-band applications. The designed structure is realized on a cost-effective, high-loss FR-4 substrate with a compact dimension. The proposed design is suitable to serve in the 5G new radio (NR) n79 (4.4 - 5 GHz), n102 (5.925 - 6.425 GHz), n104 (6.425 - 7.125 GHz) bands, as well as WLAN applications for the frequency ranges of 4.9 GHz, 5 GHz, and 5.9 GHz. The entire footprint of the designed antenna is 46 mm $\times$ 46 mm $\times$ 1.6mm. All four radiating elements are orthogonally placed, and each is coupled to a feedline for better coupling performance. To decrease the inter-element coupling among the radiators, parasitic elements are added between the patch elements. Also, a defective ground structure is used to improve isolation. These also enhance the overall antenna performance, as the result shows improvement in average isolation, total efficiency (>80%), and gain (>5 dB). The antenna design is carried out to meet the requirements of the specified frequency bands, rendering it an effective choice for WLAN, 5G NR (n79, n102, and n104), and C-band applications.

Keywords: MIMO antenna, WLAN, defected ground structure (DGS), isolation enhancement, 5G NR, C-band.

PACS: 84.40.Ba, 88.80.ht, 85.50.-n, 84.40.Dc

1 Introduction

As wireless communication technologies continue to advance, the demand for improved data rates, higher spectral efficiency, and dependable connectivity is steadily increasing. MIMO antenna technology has gained prominence as a notable development in modern communication, as it facilitates high data transfer rates, enhances spectral efficiency, and minimises signal degradation [1]. By incorporating multiple radiating elements, MIMO systems use spatial diversity and multipath propagation, thereby enabling robust performance even in complex wireless environments [2]. This technology contributes significantly in fulfilling the rising need for high-speed, reliable, and energy-efficient communication, particularly in applications such as 4G, 5G, and beyond. Consequently, MIMO has become an indispensable solution for next-generation wireless networks, where efficiency and robust connectivity are of paramount importance.

Compactness is one of the essential design considerations in MIMO antennas, especially for portable and integrated communication devices [3]. However, reducing the physical dimensions of antenna elements often results in increased mutual coupling and reduced isolation, which adversely affect the system performance as a whole. Achieving a balance between miniaturization and sufficient port isolation remains a significant challenge for antenna designers, particularly due to multiple radiating elements [1].

Various isolation enhancement techniques such as defected ground structure (DGS) method [4–6], electromagnetic bandgap (EBG) [7], balanced open slot [8], different radiating modes [9], decoupling circuits [10, 11] neutralization line (NL) [12, 13], etc. have been applied to reduce the interactions and interdependence between the radiating elements with isolation enhancement among them. Among these, DGS has been observed as a highly effective method, as it disrupts the surface current distribution and suppresses coupling paths without significantly increasing antenna size [3]. This makes DGS-based designs attractive for compact, high-performance MIMO systems.

Given these facts, researchers have been trying to develop MIMO antenna systems for different wireless applications. A MIMO antenna containing eight elements for a 5G mobile application is presented in ref. [14]. The high-performance antenna operated over the frequency range from 2.5-3.6 GHz. The antenna provided a channel capacity of 34.25 bps/Hz with 20 dB of SNR in free space, about three times that of 2×2 MIMO operations [14]. A multi-purpose dual MIMO system, comprises two MIMO antenna sets integrated on a single substrate, one 8-element MIMO with a dimension of 150 mm$\times$70 mm working on the 3.4 - 3.6 GHz frequency and one 4-port MIMO working on 5.02 - 6.93 GHz with a dimension of 20mm$\times$7mm, for 5G mobile systems, is presented in [15]. In [16], a chain of defected ground structures is used to design a MIMO antenna with low mutual coupling and minimize cross-polarization. The reported radiation efficiency was 74%, with 2 dBi peak gain. A circularly polarized MIMO antenna with orthogonal modes for the 5G cellular application system operating below 6 GHz is presented, covering the 3.4 - 3.8 GHz band [17]. The antenna design achieved more than 20 dB isolation among the elements. The overall efficiency of the suggested design was above 80%, with more than 4 dBic of CP gain in the operating bandwidth. A novel method for decoupling, by employing multiple radiation modes with varying patterns and polarizations is proposed in ref. [9]. The antenna delivered an isolation of 23 dB between 2.4 GHz and 2.65 GHz with a maximum efficiency of 92% over the operating frequency range. A small-sized dual-element MIMO antenna operating in the sub-6 GHz band for 5G applications is designed by Mathew et al. in [18]. The antenna design was based on slot radiators and used FR4 substrate. The proposed design is optimized by using a defective ground structure to increase the port-isolation. The operational bandwidth of the antenna ranges from 3.1 GHz to 4.2 GHz. In [19], Ding et. al. designed a MIMO antenna using a parabolic reflector along with a parasitic strip. The entire footprint of the compact broadband MIMO antenna element is 36mm$\times$27mm$\times$0.8 mm, printed using expensive Rogers substrate to cover the bandwidth range of 2.32 GHz to 2.95 GHz.

The works documented in the literature have employed various methods to increase isolation between radiating elements. However, the recent literature hardly ever shows low mutual coupling with high gain and overall improved antenna parameters in the case of a small antenna configuration. In these respects, the presented work features a 4-port MIMO antenna design employing a low-cost substrate for WLAN, 5G NR (n79, n102, and n104), and C-band applications. Unlike many previously reported FR-4-based MIMO antennas that achieve either wide bandwidth, high isolation, or good radiation performance at the expense of the others, the proposed design simultaneously realizes wideband operation from 4 to 8 GHz, enhanced inter-element isolation, and stable radiation characteristics within a compact footprint. Methods such as partial ground structure and parasitic elements are applied to lower the coupling to minimize the degradation of MIMO antenna performance. The antenna design achieves high isolation, large impedance bandwidth, and reliable diversity performance, rendering it a strong choice for next-generation wireless communication systems. The designed antenna structure is analyzed in terms of S-parameters, and different diversity parameters validating its suitability for practical deployment.

2 Design Methodology

2.1 Single Antenna Element:

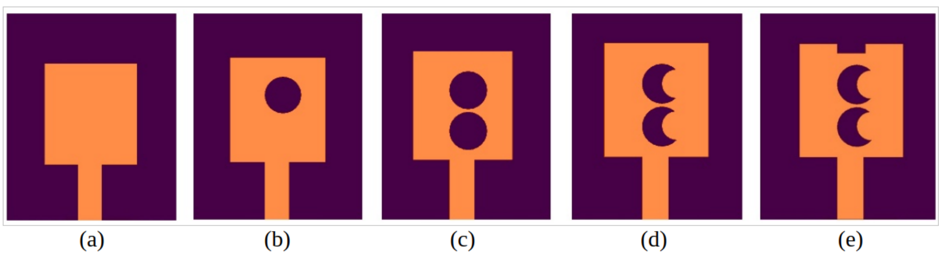

Figure 1: Evolution of single antenna element.

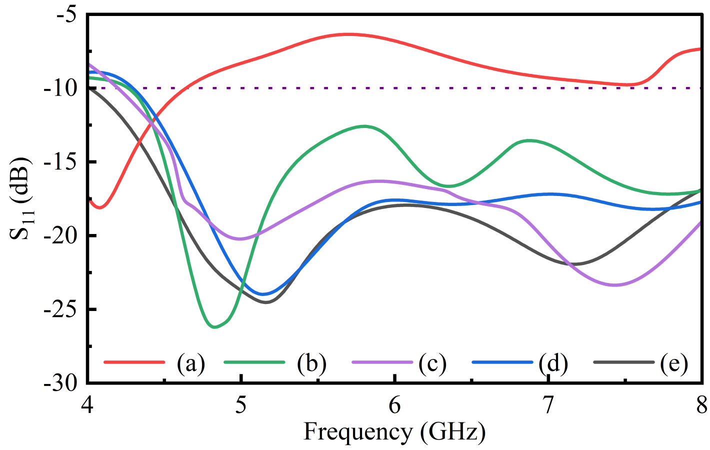

Figure 2: Variation of S11 of the antenna.

The antenna design process began with a conventional rectangular microstrip patch antenna, which serves as the reference structure due to its simple geometry and well-established characteristics. However, the basic rectangular configuration is typically constrained by limitations such as limited frequency coverage, reduced impedance matching, limited gain, and flexibility. Hence, geometrical modifications are introduced as shown in the Fig. 1. Fig. 2 shows the changes in the reflection coefficient value with the evolution of the antenna. The designed structure is implemented using cost-effective FR-4 substrate.

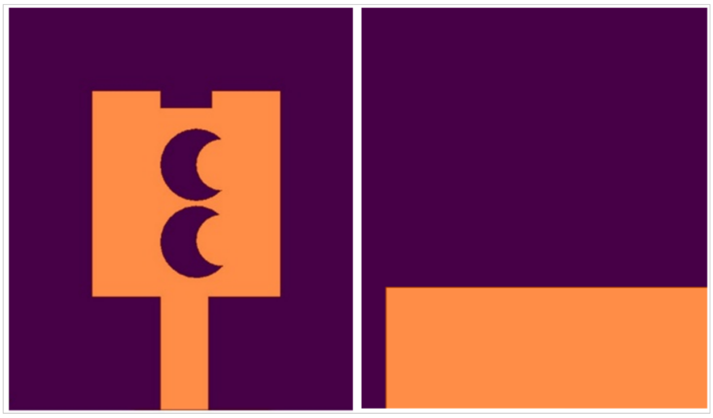

(a) Top side (b) Bottom side

Figure 3: The single antenna element.

Fig. 3 displays the single-element structure of the proposed MIMO as well as the arrangement of the design geometry of the ground plane. Each radiating patch consists of two half-moon-shaped structures with a rectangular cut on the top plane of the structure. The modified rectangular patch is fed by a microstrip feedline. For the ground plane, a partial ground structure is adopted, which helps in reducing mutual coupling and enhancing isolation. Its dimensions are designed and optimized using the `ANSYS HFSS` (High Frequency Structure Simulator) software. Fig. 4 displays the S_{11} graph for the final single antenna element.

2.2 Quad-Element MIMO Design:

Fig. 5 presents the detailed geometry of the designed MIMO design, presenting the radiating elements and ground structure along with their corresponding design parameters. The initially designed single-antenna patch is positioned orthogonally to develop a four-port MIMO antenna as illustrated in Fig. 5(a). The parasitic elements used between each of the orthogonally arranged element helps to decrease the electromagnetic coupling between the

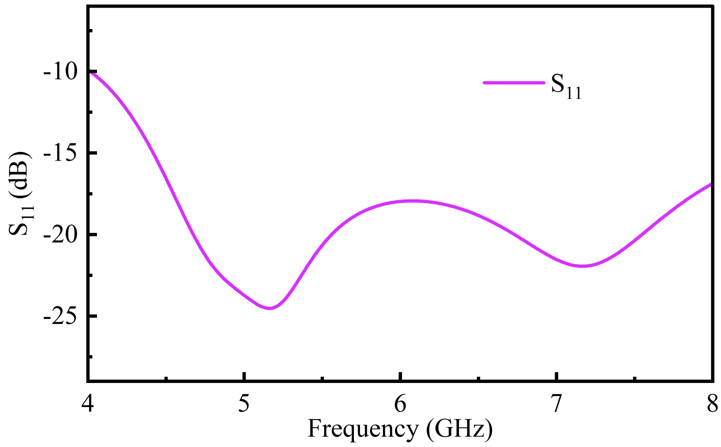

Figure 4: Return loss of the single antenna element.

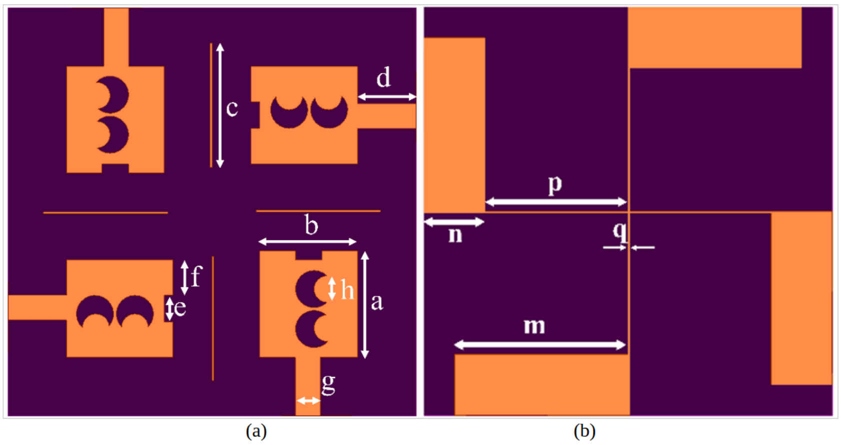

Figure 5: (a) Front and (b) back view of the 4-port MIMO.

present antenna components and suppress near-field coupling between adjacent radiators. The partial ground plane approach is adopted for the ground plane to increase the operational bandwidth of the design and disrupts surface current propagation [2]. A common reference level (common ground) is obtained by connecting the partial ground plane structures of all four ports with two thin neutralization lines, as seen in Fig. 5(b). Along with the partial ground plane structure and parasitic elements, neutralization lines are also implimented into the ground plane to lower the coupling and boost isolation. Table 1 displays the geometric dimensions of the planned structure.

Variables	**Dimensions**	**Variables**	**Dimensions**	**Variables**	**Dimensions**
a	12	e	3	m	15
b	11	f	4	n	6
c	14	g	3.2	p	12
d	6.6	h	2.9	q	0.2

Table 1: Geometric antenna variables with dimensions (in mm).

2.3 Field Distribution Analysis:

The electric and magnetic field distributions of the designed structure are presented in Fig. 6(a) and (b), respectively. Fig. 6(a) illustrates that when one port is excited, the strongest current concentration is observed around the excited radiating element. The high-intensity regions correspond to the areas of maximum electric field strength, while the gradual transition to blue regions indicates weaker fields along the ground plane and adjacent structures.

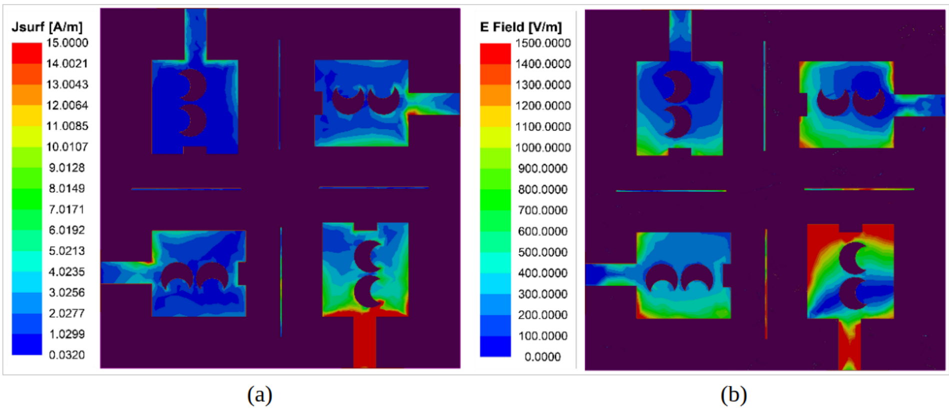

Figure 6: Surface current distribution of the design, (a) E-field and (b) H-field.

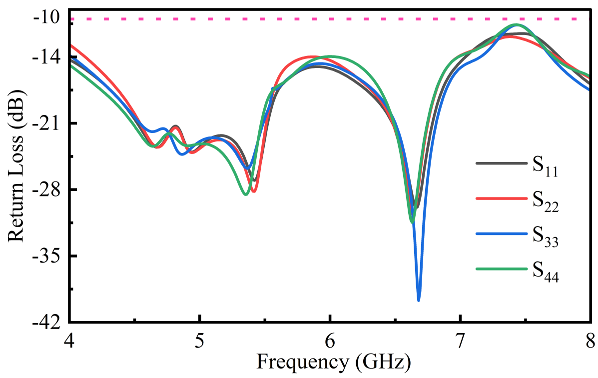

Figure 7: Return loss values of the 4-port MIMO.

The magnetic field distribution of the design structure is presented in Fig. 6(b), highlighting the concentration of the magnetic field around the current paths along the radiating elements. It can be observed that the maximum H-field intensity is concentrated near the feed and the excited radiating patch, confirming the effective excitation and radiation of the element. In addition, weaker magnetic field levels are observed around the non-excited elements, demonstrating the reduced field coupling between the ports. The application of the DGS effectively alters the field distribution and mitigates undesired interactions, thereby improving the isolation and stability of the designed compact MIMO antenna structure.

3 Results and Discussion

The acquired results from the simulation are analysed in this section. The reflection coefficients (S_{11}, S_{22}, S_{33}, and S_{44}) of the designed structure are presented in Fig. 7. The design covers the frequency range from 4 - 8 GHz. The S-parameters at ports 1, 2, 3, and 4 are -31.487 dB, -30.75 dB, -40.55 dB, and -31.76 dB, respectively. The reflection coefficient plot confirms that the antenna resonates around 5.45 GHz and 6.65 GHz, covering the desired frequency band with good impedance matching. The proposed antenna demonstrates strong return loss performance, achieving significantly higher reflection coefficient values (max. 35 dB) near the resonant frequencies. The plotted transmission coefficients indicate that the minimum (worst-case) port-to-port isolation remains better than -11.5 dB across the entire 4-8 GHz band, indicating efficient transmission and minimal reflection.

Fig. 8 presents the obtained transmission coefficients used to find the isolation among the antenna components. After using the parasitic elements, the value of isolation improved over -11.5 dB. The peak gain of the antenna is observed to be 7 dB with an efficiency greater than 80%, as presented in Fig. 9.

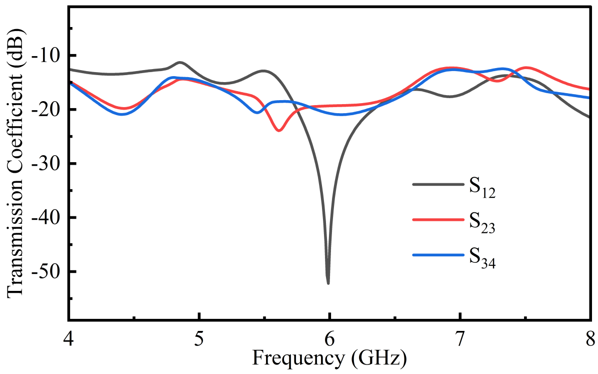

Figure 8: Transmission coefficients of the antenna.

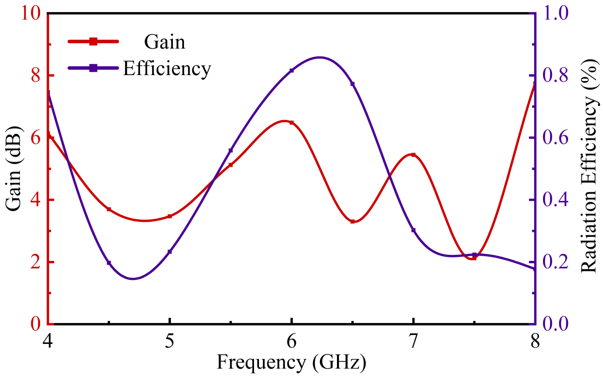

Figure 9: Gain and Efficiency of the Configuration.

4 MIMO Performance Parameters

Several diversity parameters are used to assess the performance of MIMO systems. One key metric for evaluating the interaction between radiating elements is the envelope correlation coefficient (ECC), which directly influences the channel capacity of the wireless configuration. Fig. 10 shows the calculated correlation of the proposed antenna, which is less than 0.011. Diversity gain (DG) is another important parameter that quantifies the improvement in signal reliability achieved through diversity techniques and reflects the effective reduction in transmission power requirements. It is given by the formula [1],

$$DG = 10\sqrt{1 - ECC} \tag{1}$$

and the DG value is found to be greater than 9.9992 dB.

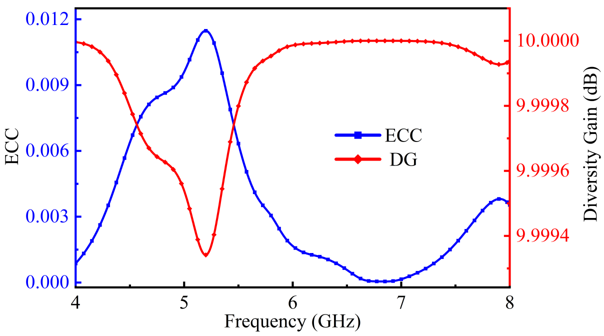

Figure 10: ECC and DG plots of the antenna.

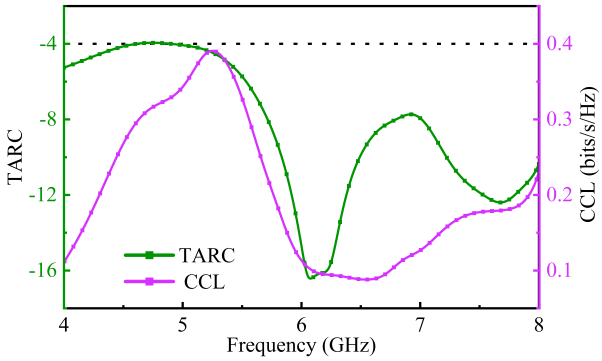

Figure 11: CCL and TARC plots of the design.

Another essential performance metric among the MIMO parameters is channel capacity loss (CCL). The suggested antenna design ensured less than 0.38 bits/s/Hz CCL value. TARC is used to verify the performance of a MIMO antenna by expressing the total incident power to the radiated power of the antenna. The TARC number should be ≤ 0 to emit the entire quantity of power properly [20]. Here, the CCL and TARC values of the introduced structure are presented in Fig. 11. These parameters are widely employed to ensure optimal system performance, as they provide insights into power distribution, mutual coupling effects, and overall channel efficiency.

All results are based on full-wave electromagnetic analysis because the goal of this work is to define the design process and validate the designed antenna structure through simulation. To verify the simulated performance empirically, the antenna will be manufactured and then measurement will be done using a VNA. Certain tolerances and material differences may have a little impact on the final performance during the practical manufacture of the suggested design, and manufacturing tolerances may cause variations in the copper cladding thickness. Small changes in the mutual coupling and slight differences in isolation may result from such adjustments. Furthermore, extra losses during measurement may be introduced by the parasitic effect caused by soldering flaws and SMA connectors. Slight variations in performance can also be brought on by environmental elements like humidity and temperature. These factors were taken into consideration during the design optimization process, and following the fabrication of prototypes and experimental characterization, they will be further investigated.

Table 2 comprises the performance characteristics of the proposed antenna structure and the various antenna structures mentioned in the literature.

Ref.	Substrate	Frequency (GHz)	Gain (dB)	Efficiency (%)	ECC	DG (dB)	TARC	CCL (bits/s/Hz)
[6]	FR-4	1.6–4.4	5.62	53	0.001	9.9	–	0.4
[9]	F4B	2.4–2.65	9.25	92	0.05	–	–	–
[21]	FR-4	3.78–9.5	3.78	81	0.04	9.997	–	–
[22]	FR-4	3.81–7.48	4.6	–	0.01	–	-10	0.4
[23]	FR-4	5.68–8.01	2.5–6.5	90	0.001	–	–	–
[24]	FR-4	2–5.2	6.3	–	0.01	10	-20	0.05
[25]	Rogers RT 5870	5.65–6.55	5.2	–	0.046	–	–	0.0758
[26]	Rogers-5880	5.2–5.7	3.05	90	0.007	9.96	-10	0.4
[27]	Rogers-5880	3.08–7.75	8.3	73–84	0.004	9.98	–	–
This work	**FR-4**	**4–8**	**7**	**87**	**0.011**	**9.9992**	**-16**	**0.38**

Table 2: Performance comparison of the designed MIMO with recent works.

5 Conclusion

The proposed work presents a small-sized quad-element MIMO design for 5G wireless applications. The prototype of the antenna structure is designed and optimized using a cost-effective FR-4 substrate. For the reduction of inter-element coupling partial ground structure is used. The MIMO design comprises four radiating patches facing each other. Each contains two half-moon shaped structure with a rectangular cut at the top of the radiating element. The defected ground structure method and the neutralization line are introduced to decrease the inter-element interaction between the radiating components. The designed antenna also uses parasitic elements for the same purpose. This approach enhances isolation between the radiating elements as isolation coefficients are less than -11.5 dB. The value of ECC is found to be less than 0.011, indicating that the coupling of the antenna is very low. The value of CCL is 0.38 bits/s/Hz. In addition, diversity gain is greater than 9.9992. These characteristics make the proposed antenna structure well-suited for the 5G NR n79, n102, and n104 bands. The present work is limited to the design and full-wave simulation of a four-element antenna structure. Fabrication and measurement of the designed antenna will be carried out in future studies to provide experimental validation of the simulated performance.

Acknowledgements

The authors sincerely acknowledge the DST FIST (level-I) Project No (SR/FST/PSI-217/2016) and the DST PURSE Project No (SR/PURSE/2022/143) and funding by Department of Science Technology, Govt. of India to the Department of Physics, Dibrugarh University, Assam, India.

References

[1] A. C. Balanis and D. R. Cockrell, IEEE Trans. Aerosp. Electron. Syst. **AES-7**, 960 (1971).

[2] M. Alibakhshikenari *et al.*, Sci. Rep. **12**, 7907 (2022).

[3] V. K. Gupta and R. Baru, in *Advances in Intelligent Computing and Communication. Lecture Notes in Networks and Systems, Vol. 202*, edited by S. Das and M. N. Mohanty (Springer, Singapore, 2021), pp. 199–209.

[4] H. Xing *et al.*, Electronics **9**, 1265 (2020).

[5] T. Doloi *et al.*, in *2024 15th International Conference on Computing Communication and Networking Technologies (ICCCNT)* (2024), pp. 1–6.

[6] G. Shankar Das *et al.*, Mater. Today Proc. (2023), *article in press*.

[7] W. Wu, B. Yuan and A. Wu, Int. J. Antennas Propag. **2018**, 8490740 (2018).

[8] Y. Li *et al.*, IEEE Trans. Antennas Propag. **67**, 3820 (2019).

[9] Y.-F. Cheng and K.-K. M. Cheng, IEEE Trans. Antennas Propag. **69**, 8204 (2021).

[10] H. Jiang *et al.*, in *2019 International Conference on Microwave and Millimeter Wave Technology* (ICMMT, 2019), pp. 1–3.

[11] W. Hu *et al.*, IEEE Access **7**, 153910 (2019).

[12] A. A. Megahed *et al.*, IEEE Access **10**, 19875 (2022).

[13] A. Birwal *et al.*, MAPAN **36**, 763 (2021).

[14] M. Abdullah, S. H. Kiani and A. Iqbal, IEEE Access **7**, 134488 (2019).

[15] P. Mathur *et al.*, IEEE Access **9**, 106734 (2021).

[16] J. Acharjee, K. Mandal and S. K. Mandal, AEU–Int. J. Electron. Commun. **97**, 110 (2018).

[17] S. Chakraborty *et al.*, SN Appl. Sci. **2**, 1180 (2020).

[18] S. Mathew, G. Saini and S. S. Gill, Int. J. Recent Technol. Eng. **9**, 202 (2020).

[19] K. Ding *et al.*, IEEE Antennas Wireless Propag. Lett. **16**, 2349 (2017).

[20] T. Doloi *et al.*, Phys. Scr. **99**, 105013 (2024).

[21] N. Das *et al.*, in *2023 International Conference on Electrical, Computer and Communication Engineering (ECCE)*, (IEEE, 2023), pp. 1-6.

[22] B. M. Yousef *et al.*, AEU–Int. J. Electron. Commun. **170**, 154815 (2023).

[23] Z. Wang, M. Wang and W. Nie, Electronics **12**, 3465 (2023).

[24] S. Hassan Ghadeer *et al.*, AEU–Int. J. Electron. Commun. **159**, 154480 (2023).

[25] M. Mishra *et al.*, IEEE Access **10**, 49829 (2022).

[26] A. Ali *et al.*, Ain Shams Eng. J. **15**, 102579 (2024).

[27] M. M. Hasan *et al.*, Sci. Rep. **12**, 9433 (2022).